

Quantization of Fractional Corner Charge in C_n -symmetric Topological Crystalline Insulators

Vladimir A. Benalcazar, Tianhe Li, and Taylor L. Hughes

Department of Physics and Institute for Condensed Matter Theory,

University of Illinois at Urbana-Champaign, IL 61801, USA

(Dated: March 8, 2022)

We show that C_n symmetries quantize the corner charge in crystalline topological insulators. We classify two-dimensional crystalline insulators having time-reversal and C_n symmetries and construct sets of primitive generator models that span these classifications. From these generators we are able to characterize the existence of corner fractional charge systematically and relate it to the symmetry representations of the occupied energy bands. We find that C_4 , C_3 , and C_6 symmetric crystalline insulators have fractional corner charges in multiples of $\frac{e}{4}$, $\frac{e}{3}$, and $\frac{e}{6}$, respectively. C_2 symmetry, on the other hand, does not protect the fractional quantization of corner charge. Our findings are compiled in a set of topological indices that quantify the amount of charge robustly localized at corners. When an additional chiral symmetry is present, $\frac{e}{2}$ corner charges are accompanied by zero-energy corner-localized states. Finally, we discuss the role of fractional charges bound to disclinations as bulk probes for these topological insulators.

Crystalline insulators with a bulk dipole moment have surface charge densities equal to the their dipole moment density [1–3]. Additionally, crystalline insulators with higher bulk multipole moments have lower order moments bound to their boundaries [4, 5]. Thus, for example, a quadrupole insulator has edge-bound dipole moments and corner-bound charges, while an octupole insulator has surface-bound quadrupole moments, hinge-bound dipole moments, and corner-bound charges. An alternative mechanism for the existence of corner charges is the presence of edge-localized dipole moments that converge at a corner [5, 6]. While higher multipole moments can lead to the quantization of fractional charge in the presence of certain C_n symmetries [5], in this paper we show that C_n symmetric insulators with vanishing bulk electric moments can also have non-vanishing quantized fractional corner charge.

A well-defined corner charge exists only if its bulk dipole moment identically vanishes, as otherwise the symmetry-preserving edges of the sample are metallic and would delocalize the corner charge. The quantization of corner charge therefore has to be associated with new topological indices. We derive these indices and write them in terms of rotation invariants which we define. These indices (along with the requirement that the indices for bulk dipole moment vanish), indicate the corner-bound charge quanta given a C_n symmetry. We find that, in general, the emergence of fractional charge is a collective effect of the bulk states and is not always accompanied with spectrally isolated corner-bound states. For C_n symmetric insulators that additionally exhibit chiral symmetry, however, the presence of $\frac{e}{2}$ corner charge is associated with the existence of gapless corner-bound states which allows for a spectroscopic identification.

In our study, we first classify 2D crystalline insulators in class AI having additional C_n symmetry. The topological classes are indicated by sets of rotation topological

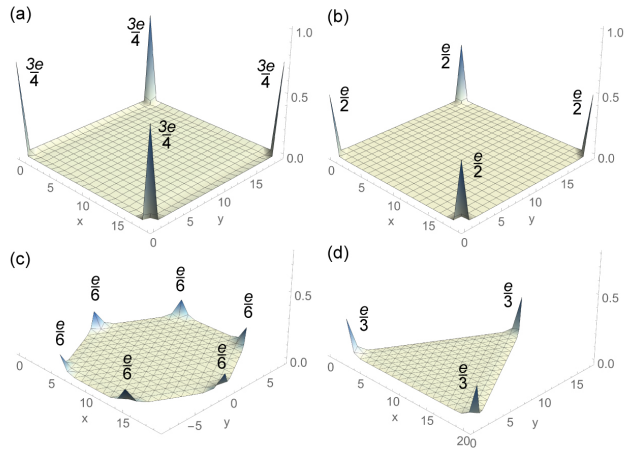


FIG. 1: Quantized fractional corner charge in C_n symmetric insulators. The plots show the total (electronic and ionic) charge density of two-dimensional TIs with open boundary conditions along all directions for (a) a C_4 symmetric TI with electronic corner charge $\frac{e}{4}$, (b) a C_4 symmetric TI with electronic corner charge $\frac{e}{2}$, (c) a C_6 symmetric TI with electronic corner charge $\frac{5e}{6}$, and (d) a C_3 symmetric TI with electronic corner charge $\frac{2e}{3}$. In all cases, the bulk *and* edges are neutral.

invariants. We then present model Hamiltonians that constitute *primitive generators* that span these classifications. Our primitive generators are in nontrivial obstructed atomic limits having Wannier centers at maximal Wyckoff positions of the unit cell fixed by C_n symmetry. By identifying the edge and corner charge arising from all inequivalent Wyckoff positions, we use an algebraic method to combine our primitive generators in order to relate the sets of rotation topological invariants to the quanta of corner fractional charge.

We find that C_4 , C_3 , and C_6 symmetric crystalline insulators have fractional corner charges in multiples of $\frac{e}{4}$, $\frac{e}{3}$, and $\frac{e}{6}$, respectively, as shown in Fig. 1. C_2 symme-

try, on the other hand, does not protect the fractional quantization of corner charge.

Classification. – Two-dimensional crystalline insulators in class AI [7–9] preserve time-reversal symmetry (TRS), having Bloch Hamiltonians satisfying $h(\mathbf{k}) = h^*(-\mathbf{k})$. These systems have a vanishing Hall conductance, indicated by a zero Chern number. The presence of additional C_n symmetry, however, allows for a finer classification nontrivial topological phases in these insulators [10–13]. These classes can be most directly distinguished by the value of their polarization [1, 2]

$$\mathbf{P} = p_1 \mathbf{a}_1 + p_2 \mathbf{a}_2, \quad (1)$$

where \mathbf{a}_1 and \mathbf{a}_2 are primitive unit lattice vectors and the components p_1 and p_2 are topological indices that correspond to quantized Berry phases along the non-contractible loops of the Brillouin zone (BZ) [11, 14–16]. We take \mathbf{a}_1 and \mathbf{a}_2 to be $\mathbf{a}_1 = \hat{\mathbf{x}}$, $\mathbf{a}_2 = \hat{\mathbf{y}}$ in C_4 and C_2 symmetric lattices and $\mathbf{a}_1 = \hat{\mathbf{x}}$, $\mathbf{a}_2 = \frac{1}{2}\hat{\mathbf{x}} + \frac{\sqrt{3}}{2}\hat{\mathbf{y}}$ in C_6 and C_3 symmetric lattices (note that we have set all lattice constants to unity). As shown in the Supplementary Information (SI), the values of the polarization \mathbf{P} form a \mathbb{Z}_2 index in C_4 -symmetric insulators, a $\mathbb{Z}_2 \times \mathbb{Z}_2$ index in C_2 -symmetric insulators, and \mathbb{Z}_3 index in C_3 -symmetric insulators; while in C_6 symmetric insulators the polarization always vanishes.

More generically, we can distinguish nontrivial topological classes arising from the C_n symmetry through the symmetry representations that the occupied energy bands take at the high symmetry points of the BZ (HSPs) [10–13, 17, 18]. Consider C_n -symmetric Bloch Hamiltonians, which obey $\hat{r}_n h(\mathbf{k}) \hat{r}_n^\dagger = h(R_n \mathbf{k})$, where \hat{r}_n is the n -fold rotation operator having $\hat{r}_n^n = 1$ and R_n is the n -fold rotation matrix acting on the crystal momentum \mathbf{k} . We denote the HSPs as $\mathbf{\Pi}^{(n)}$. These are defined as the special points in the BZ which obey $R_n \mathbf{\Pi}^{(n)} = \mathbf{\Pi}^{(n)}$ modulo a reciprocal lattice vector. Rotation symmetry then implies that $[\hat{r}_n, h(\mathbf{\Pi}^{(n)})] = 0$. Thus, the energy eigenstates of the Bloch Hamiltonian are also eigenstates of the rotation operator. Let us denote the eigenvalues of \hat{r}_n at HSP $\mathbf{\Pi}^{(n)}$ as

$$\Pi_p^{(n)} = e^{2\pi i(p-1)/n}, \quad \text{for } p = 1, 2, \dots, n. \quad (2)$$

Given a subspace of energy bands, we can compare these rotation eigenvalues at the various HSPs. If different representations (sets of eigenvalues) of a rotation symmetry exist at different HSPs, the energy bands in question have nontrivial topology (here we include obstructed atomic limits in our definition of topological). Accordingly, we use the rotation eigenvalues at momenta, $\mathbf{\Pi}^{(n)}$ compared to a reference point $\mathbf{\Gamma} = (0, 0)$, to define the integer topological invariants

$$[\Pi_p^{(n)}] \equiv \#\Pi_p^{(n)} - \#\Gamma_p^{(n)}, \quad (3)$$

where $\#\Pi_p^{(n)}$ is the number of energy bands below the energy gap with eigenvalue $\Pi_p^{(n)}$. Not all these invariants are independent, however. First, rotation symmetry can force representations at certain HSPs to be the same. C_4 symmetry forces the representations at \mathbf{X} and \mathbf{X}' in the BZ to be equal, while C_6 symmetry forces equal representations at \mathbf{M} , \mathbf{M}' , and \mathbf{M}'' , as well as at \mathbf{K} and \mathbf{K}' . Furthermore, there are redundancies in the invariants due to: (i) the fact that the number of bands in consideration is constant across the BZ, from which it follows that $\sum_p \#\Pi_p^{(n)} = \sum_p \#\Gamma_p^{(n)}$, or $\sum_p [\Pi_p^{(n)}] = 0$, and (ii) the existence of TRS, which implies that rotation eigenvalues at $\mathbf{\Pi}^{(n)}$ and $-\mathbf{\Pi}^{(n)}$ are related by complex conjugation. This results in the relations $[M_2^{(4)}] = [M_4^{(4)}]$, $[K_2] = [K_3']$, and $[K_3] = [K_2']$. Dropping the redundant invariants due to these constraints, the resulting topological classes of crystals with C_n symmetry are given by the indices $\chi^{(n)}$, as follows,

$$\begin{aligned} \chi^{(4)} &= ([X_1], [M_1^{(4)}], [M_2^{(4)}]) \\ \chi^{(2)} &= ([X_1], [Y_1], [M_1^{(2)}]) \\ \chi^{(6)} &= ([M_1], [K_1]) \\ \chi^{(3)} &= ([K_1], [K_2]). \end{aligned} \quad (4)$$

We also note that the C_2 invariants of a C_4 symmetric insulator obey $[X_1] = [Y_1]$ and $[M_1^{(2)}] = -2[M_2^{(4)}]$, and the C_3 invariants of a C_6 symmetric insulator obey $[K_1] = [K_2]$. Two C_n -symmetric crystals are stably equivalent if and only if they have the same topological invariant $\chi^{(n)}$ [12, 13, 19, 20]. C_n symmetric insulators with different $\chi^{(n)}$, on the other hand, belong to different topological classes, as they cannot be deformed into one another without closing the bulk energy gap or breaking the symmetry.

Having identified the quantities that distinguish the C_n protected topological phases we can apply the algebraic method developed in Refs. 12, 13 to connect the representation invariants to physical properties. The topological classification $\chi^{(n)}$ forms a free Abelian additive structure. Two C_n -symmetric insulators with Hamiltonians $h_1^{(n)}$ and $h_2^{(n)}$, in classes $\chi_1^{(n)}$ and $\chi_2^{(n)}$, and having rotation operators \hat{r}_n and \hat{r}'_n , respectively, can be stacked leading to a third C_n -symmetric insulator with Hamiltonian $h_3^{(n)} = h_1^{(n)} \oplus h_2^{(n)}$ and with rotation operator $\hat{r}_n'' = \hat{r}_n \oplus \hat{r}'_n$. The resulting insulator is in class $\chi_3^{(n)} = \chi_1^{(n)} + \chi_2^{(n)}$. Thus, given a C_n symmetry which classifies insulators using N topological invariants, all topological classes in that classification, and their resulting physical topological observables, can be accessed by a set of N primitive generators: sets of C_n -symmetric insulators having invariants represented by vectors $\chi^{(n)}$ which are linearly independent to one another. From the classifications in Eq. 4, it follows that all stable topological classes can be accessed by sets of 3 primitive generators

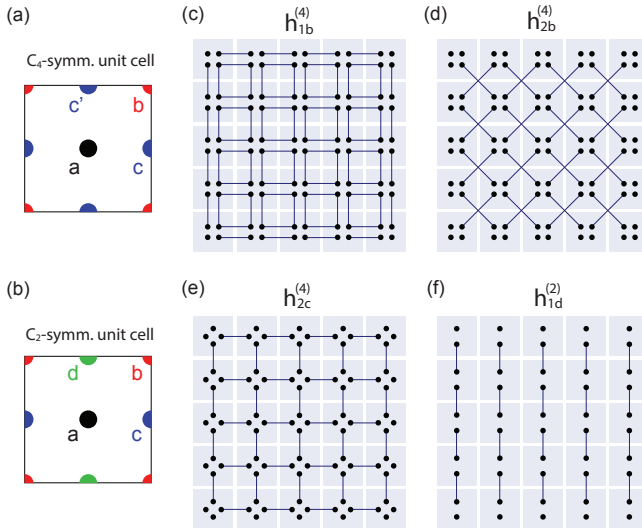


FIG. 2: (a,b) Maximal Wyckoff positions for (a) C_4 - and (b) C_2 -symmetric unit cells. (c-e) Lattices for the three primitive generators that span the classification of C_4 -symmetric insulators. The lattices for the primitive generators for the classification of C_2 -symmetric insulators are those in (c), (e), and (f).

for each of the classifications of C_4 and C_2 symmetric TIs and by 2 primitive generators for each of the classifications of C_6 and C_3 symmetric TIs.

Primitive generators. – The primitive generators we consider are illustrated in Figs. 2 and 3. All the generators are insulators that admit a Wannier representation [21, 22] of their occupied bands. To span the classifications, these generators have nontrivial topology, captured by nonzero $\chi^{(n)}$ invariants, as indicated in Table I. In the bulk, the nontrivial topology of these generators manifest in that their Wannier centers are pinned, by symmetry, to maximal Wyckoff positions other than at the center of the unit cell. In contrast, trivial bands will necessarily have Wannier centers at the center of the unit cell [position 1a marked with black dots in Figs. 2(a,b) and 3(a,b)], which coincide with the position of the atomic centers. We will refer to this trivial configuration as the *trivial atomic limit*. Insulators with a trivial topology can always be deformed into the trivial atomic limit without closing the energy gap. Insulators with Wannier configurations at other Wyckoff positions enforced by symmetries, as our primitive generators, are in *obstructed atomic limits* [17], because a connection to the trivial atomic limit is not allowed unless a gap-closing phase transition occurs or the symmetry is broken. Although pictured in their simplest forms in Figs. 2 and 3, adding on-site hopping terms, or other symmetry-allowed terms, to our generators can transition them into a variety of phases in their respective $\chi^{(n)}$ classifications. The analysis of some of the phases of the generator models is deferred to the SI. Instead, we focus on the limits in

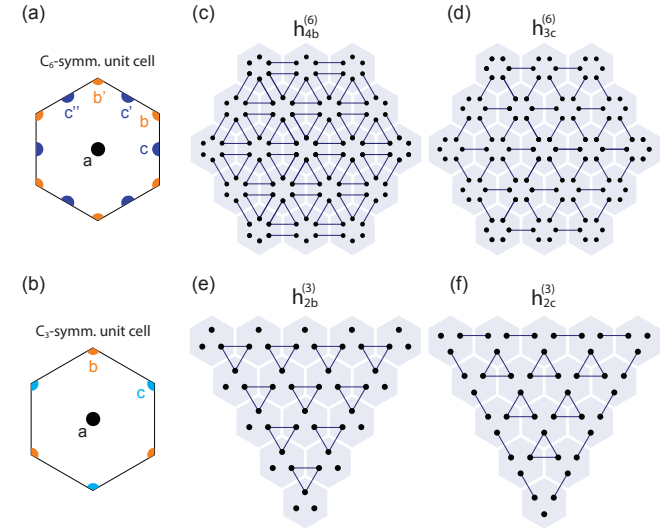


FIG. 3: (a,b) Maximal Wyckoff positions for (a) C_6 - and (b) C_3 -symmetric unit cells. (c,d) Primitive generators than span the classification of C_6 -symmetric insulators. (e,f) Primitive generators for the classification of C_3 -symmetric insulators.

which onsite hopping terms are zero because they allow us to pictorially infer the locations of the Wannier centers, and these will not change away from the zero correlation length limit.

Let us know describe the primitive generator models. We use the notation that a generator $h_{mW}^{(n)}$ is C_n symmetric, it has m filled bands, and has Wannier centers at the maximal Wyckoff positions W shown in Figs. 2 (a,b) and 3 (a,b). The classification of C_4 -symmetric TIs has three generators: $h_{1b}^{(4)}$, $h_{2b}^{(4)}$, and $h_{2c}^{(4)}$ [Fig. 2(c,d,e)]. All of them have four energy bands. The lattice model in Fig. 2(c) has a gap that separates the first and the second bands and another one that separates the third and four bands. We take the first generator $h_{1b}^{(4)}$ to occupy only the lowest band, i.e., $\frac{1}{4}$ -filling. The generators $h_{2b}^{(4)}$, and $h_{2c}^{(4)}$ are gapped at half filling; hence, we take both of these generators to occupy the lowest two bands. As indicated by their labels, the first two generators have one and two Wannier centers at the position b , respectively [red dot in Fig. 2(a)], while the third generator has Wannier centers at the two inequivalent positions c and c' [blue dots in Fig. 2(a)].

The classification of C_2 -symmetric TIs also requires three generators. We choose the first two of them to be $h_{1b}^{(4)}$ and $h_{2c}^{(4)}$ [Fig. 2(c,e)]. The generator $h_{2b}^{(4)}$ is not independent because its C_2 invariants are given by the vector $\chi^{(2)} = (2, 2, 0)$, which is linearly proportional to the invariant vector of $h_{1b}^{(4)}$, $\chi^{(2)} = (-1, -1, 0)$. Indeed, from the relation between invariants we can see that $h_{2b}^{(4)} \sim -h_{1b}^{(4)} \oplus -h_{1b}^{(4)}$. The third generator is a two-dimensional version of the SSH model [23], labeled as

$h_{1d}^{(2)}$ and shown in Fig. 2(f) in its extremely dimerized limit. As the label indicates, it is an obstructed atomic limit with Wannier center at position d .

The classification of C_6 symmetric TIs requires two generators. We take them to be $h_{4b}^{(6)}$ and $h_{3c}^{(6)}$ [Fig. 3(c,d)]. Both of them have six energy bands. $h_{4b}^{(6)}$ is taken to occupy the lowest four bands and has a pair of Wannier centers at each of the Wyckoff positions b and b' [orange dots in Fig. 3(a)], while $h_{3c}^{(6)}$ is taken to occupy the lowest three bands and has its three Wannier centers at positions c , c' , and c'' [blue dots in Fig. 3(a)].

The classification of C_3 symmetric TIs requires two generators. We take them to be $h_{2b}^{(3)}$ and $h_{2c}^{(3)}$ [Fig. 3(e,f)], which are related to each other by a rotation of π . Each of these generators has three energy bands with a degeneracy in the lowest two bands protected by C_3 and TRS at the Γ point. We therefore take these two models to occupy the lowest two energy bands. $h_{2b}^{(3)}$ has its two Wannier centers at the Wyckoff positions b [orange dot in Fig. 3(b)], while $h_{2c}^{(3)}$ has them at position c [cyan dot in Fig. 3(b)].

Edge and corner charge. – Knowing the Wyckoff positions of the electrons in the primitive generators allows us to extract their edge and corner charge configurations. In previous work, the polarization components $p_{i=1,2}$ have been related to the inversion or reflection eigenvalues that the subspace of occupied states take at the HSPs [15, 16]. In our classifications, the value of polarization can be determined from the generators and written in terms of the invariants of Eq. 4. As shown in the SI, the quantized values of polarization in terms of these invariants are

$$\begin{aligned} p_1 = p_2 = \frac{e}{2}[X_1] \} & C_4 \text{ symm.} \\ p_1 = \frac{e}{2}([Y_1] + [M_1^{(2)}]) \quad p_2 = \frac{e}{2}([X_1] + [M_1^{(2)}]) \} & C_2 \text{ symm.} \\ p_1 = p_2 = 0 \} & C_6 \text{ symm.} \\ p_1 = p_2 = \frac{2e}{3}([K_1] + 2[K_2]) \} & C_3 \text{ symm.}, \end{aligned} \quad (5)$$

all of which are defined mod e .

Now, let us focus on the corner charge. We find that $C_{n=4,6,3}$ symmetries protect quantized corner charge, while C_2 symmetry generally does not (see SI). Thus, we will not discuss the classification of C_2 symmetric TIs further. Let us illustrate how we determine the charge configurations of the generators. Figure 4 shows schematically the electronic charge distribution for configurations of electrons at the maximal Wyckoff positions for $C_{n=4,6,3}$ symmetric insulators. We pictorially account for the contribution to electronic charge in a unit cell by adding the portions of the electrons that fall into that particular unit cell [24]. The electronic configurations in Fig. 4 show bulk electrons (solid circles), but also boundary electrons (dimmed circles) that do not respect the C_n symmetry of the lattice. Unless C_n symmetry is broken,

there will always be more boundary states than electrons to fill them whenever $\mathbf{P} \neq (0,0)$. As a consequence, the dimmed electrons are really delocalized along the boundary in a metallic state if we tune away from the zero correlation-length limit. To have well defined corner charges, we will need to eventually enforce $\mathbf{P} = (0,0)$. In the meantime, however, we will continue to analyze the schematic configurations of Fig. 4. In C_4 symmetric TIs, Wyckoff positions at b [Fig. 4(a)] and at c, c' [Fig. 4(b)] both have polarization $\mathbf{P} = (\frac{e}{2}, \frac{e}{2})$. The fractional charge on the edges are due to the non-vanishing polarization. However, when we consider corners, a crucial distinction emerges from this picture; electrons at Wyckoff positions b have fractional corner charge in multiples of $\frac{e}{4}$, while electrons at positions c, c' have no fractional corner charge. In C_6 symmetric TIs, $\mathbf{P} = (0,0)$, leading to no edge charge. At corners, however, the charge is fractionalized. Wyckoff positions at b and b' [Fig. 4(c)] give corner charge in multiples of $\frac{e}{3}$, while Wyckoff positions at c, c' and c'' [Fig. 4(d)] give corner charge in multiples of $\frac{e}{2}$. In C_3 symmetric TIs, we have a similar scenario as in C_4 symmetric TIs. The configurations with Wyckoff positions at b [Fig. 4(e)] and at c [Fig. 4(f)] have polarizations of $\mathbf{P} = (\frac{2e}{3}, \frac{2e}{3})$ and $\mathbf{P} = (\frac{e}{3}, \frac{e}{3})$, respectively, which give rise to the edge charge. At corners, however, the configuration at Wyckoff position b does not have fractional charges, while the configuration at Wyckoff position c does (for triangular lattices pointing up, the boundary properties are reversed for these two configurations). By these considerations, the electronic corner charge for the primitive generators are found to be those in Table I.

With the invariants and boundary charges of our primitive models [Table I], we build index theorems that indicate the fractional corner charge in insulators in class AI. This relies on the fact that for a Hamiltonian $h_3^{(n)} = h_1^{(n)} \oplus h_2^{(n)}$, (i) its boundary charge is $Q_3 = Q_1 + Q_2 \bmod e$, and (ii) its invariants are $\chi_3^{(n)} = \chi_1^{(n)} + \chi_2^{(n)}$. The index for the corner charge of a C_n -symmetric insulator is then given by some linear combination of the invariants that form the vector $\chi^{(n)}$. For example, C_4 -symmetric insulators have three invariants. The corner charge is given by $Q_{\text{corner}} = \alpha_1[X_1] + \alpha_2[M_1^{(4)}] + \alpha_3[M_2^{(4)}]$. To find the coefficients $\alpha_{i=1,2,3}$, we solve for $Q_i = \chi_{ij}^{(4)} \alpha_j$, where Q_i is i th element in the vector of corner charges formed by the last column in Table I, and $\chi_{ij}^{(4)}$ is the (i, j) th element in the matrix formed by the three columns labeled $[X_1]$, $[M_1^{(4)}]$, and $[M_2^{(4)}]$ in Table I. This approach gives, for $C_{n=4,6,3}$ symmetric lattices,

$$\begin{aligned} Q_{\text{corner}} &= \frac{e}{4}([X_1] + 2[M_1^{(4)}] + 3[M_2^{(4)}]) \} C_4 \text{ symm.} \\ Q_{\text{corner}} &= \frac{e}{4}[M_1] + \frac{e}{6}[K_1] \} C_6 \text{ symm.} \\ Q_{\text{corner}} &= \frac{e}{3}[K_2] \} C_3 \text{ symm.} \end{aligned} \quad (6)$$

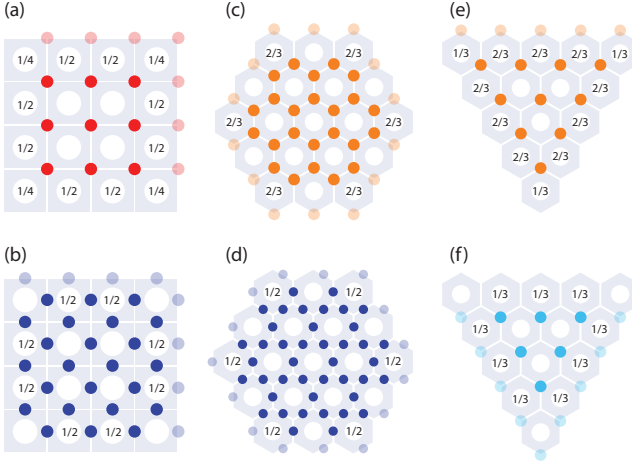


FIG. 4: Edge and corner fractional charges for crystals with Wannier centers at maximal Wyckoff positions for C_4 -symmetric lattices (a,b), C_3 -symmetric lattices (c,d), and C_6 -symmetric lattices (e,f). (a) One electron at position b . (b) Two electrons, one at position c and another one at c' . (c) Two electrons, one at position b and another one at b' . (d) Three electrons, one at position c , a second one at c' , and a third one at c'' . (e) One electron at position b . (f) One electron at position c . Solid colored circles represent bulk electrons; dimmed colored circles represent boundary electrons for a particular choice of C_n -symmetry breaking; white circles represent atomic ions. Bulk unit cells are always neutral. Electronic charges at edge and corner unit cells are indicated mod e (in units of the electron charge e).

all of which are defined mod e . In the $C_{n=4,6,3}$ symmetric classification, Q^{corner} is a \mathbb{Z}_n topological index. In the SI we discuss the generalization of these indices for the cases of having corners at other angles.

We could refer to the indices in Eq. 6 as *secondary topological indices* because they require the primary topological index — the polarization \mathbf{P} — to vanish in order to give a protected, corner-localized quantized feature. If, on the contrary, $\mathbf{P} \neq \mathbf{0}$, the edges will not be insulating and the corner charge will consequently be ill-defined generically. As an example of the application of this index, let us consider the realization of a C_4 symmetric TI with quantized electronic corner charge of $\frac{e}{4}$, having the total (electronic *and* ionic) charge density shown in Fig. 1(a). This model is the eight-band model with Bloch Hamiltonian

$$h^{(4)} = \begin{pmatrix} h_{1b}^{(4)} & \gamma_c \\ \gamma_c^\dagger & h_{2c}^{(4)} \end{pmatrix} \quad (7)$$

which couples the primitive generators $h_{1b}^{(4)}$ and $h_{2c}^{(4)}$ by the term γ_c . At $\frac{1}{4}$ filling, $h_{1b}^{(4)}$ alone has edge modes owing to its $\mathbf{P} = (\frac{e}{2}, \frac{e}{2})$ polarization. Not all the edge states are occupied at this filling, however, and the edge is metallic if the symmetry is preserved (see SI for details). We triv-

symm.	generator	Invariants			\mathbf{P}	Q^{corner}
		$[X_1] \ [M_1^{(4)}] \ [M_2^{(4)}]$				
C_4	$h_{1b}^{(4)}$	-1	1	0	$(\frac{e}{2}, \frac{e}{2})$	$\frac{e}{4}$
	$h_{2b}^{(4)}$	2	0	0	$(0,0)$	$\frac{e}{2}$
	$h_{2c}^{(4)}$	1	1	-1	$(\frac{e}{2}, \frac{e}{2})$	0
		$[X_1] \ [Y_1] \ [M_1^{(2)}]$				
C_2	$h_{1b}^{(4)}$	-1	-1	0	$(\frac{e}{2}, \frac{e}{2})$	\times
	$h_{2c}^{(2)}$	1	1	2	$(\frac{e}{2}, \frac{e}{2})$	\times
	$h_{1d}^{(2)}$	0	1	1	$(0, \frac{e}{2})$	\times
		$[M_1] \ [K_1]$				
C_6	$h_{4b}^{(6)}$	0	2		$(0,0)$	$\frac{e}{3}$
	$h_{3c}^{(6)}$	2	0		$(0,0)$	$\frac{e}{2}$
		$[K_1] \ [K_2]$				
C_3	$h_{2b}^{(3)}$	1	-1		$(\frac{e}{3}, \frac{e}{3})$	$\frac{2e}{3}$
	$h_{2c}^{(3)}$	1	0		$(\frac{2e}{3}, \frac{2e}{3})$	0

TABLE I: Topological invariants, polarization and corner charge of the primitive generators that span the classification of C_n -symmetric crystalline insulators. The values of polarization $\mathbf{P} = p_1 \mathbf{a}_1 + p_2 \mathbf{a}_2$ are given in pairs (p_1, p_2) . The unit lattice vectors are $\mathbf{a}_1 = \hat{\mathbf{x}}$, $\mathbf{a}_2 = \hat{\mathbf{y}}$ for C_4 and C_2 symmetric lattices, and $\mathbf{a}_1 = \hat{\mathbf{x}}$, $\mathbf{a}_2 = \frac{1}{2}\hat{\mathbf{x}} + \frac{\sqrt{3}}{2}\hat{\mathbf{y}}$ for C_3 and C_6 symmetric lattices.

ialize the polarization by the addition of $h_{2c}^{(4)}$, which at $\frac{1}{2}$ filling also has $\mathbf{P} = (\frac{e}{2}, \frac{e}{2})$. Under any C_4 symmetry-preserving coupling terms γ_c that keep the energy gap open, the first topological invariant of the combined insulator Eq. 7 at $\frac{3}{8}$ filling is $\mathbf{P} = (0,0)$, but its secondary index is $Q^{corner} = \frac{e}{4}$. In the SI, we add general random hopping terms to the Hamiltonian up to nearest-neighbor unit cells that preserve only TRS and C_4 symmetry and show that the $\frac{e}{4}$ charge is strictly quantized. In contrast, if we add perturbations that break C_4 symmetry down to C_2 symmetry, the quantization of the corner charge is lost (although the bulk polarization remains quantized to zero).

The indices in Eq. 6 can be used to generate other corner charges. The fractional charge of $\frac{e}{2}$ in Fig. 1(b) was obtained with a Hamiltonian deformable to $h_{1b}^{(4)} \oplus h_{1b}^{(4)}$ at $\frac{1}{4}$ filling, while the corner charges of $\frac{e}{6}$ and $\frac{e}{3}$ in Fig. 1(c,d) were obtained by Hamiltonians deformable to $h_{4b}^{(6)} \oplus h_{3c}^{(6)}$ at $\frac{7}{12}$ filling and to $h_{2b}^{(3)} \oplus h_{2c}^{(3)}$ at $\frac{2}{3}$ filling, respectively. In all cases, the polarization of the Hamiltonians is $\mathbf{P} = (0,0)$, and the corner charge indices in Eq. 6 give $Q^{corner} = \frac{e}{2}, \frac{5e}{6}$, and $\frac{2e}{3}$, respectively. The total charge density, which takes into account the ionic contributions, results in the fractional charges shown in Fig 1.

The fractionalization of corner charge is a bulk topological property of the subspace of occupied bands, and does not need to manifest corner-localized mid-gap

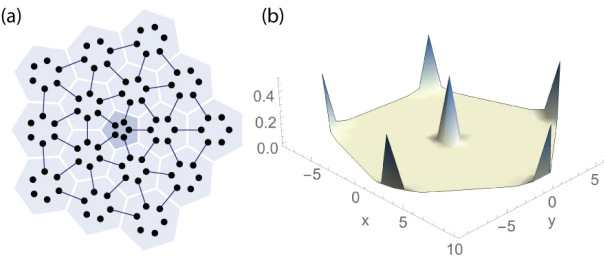


FIG. 5: Quantized fractionalization of charge at the core of disclinations. (a) Disclination in the lattice of primitive generator $h_{3c}^{(6)}$ (core of disclination is shown in darker color). (b) Charge density for the disclination in (a). All corners and the core of the disclination have charges of $\frac{e}{2}$. The simulation is done over 276 unit cells with added intra-unit cell hoppings between nearest neighbors of $\frac{1}{4}$ the amplitude of the inter-unit cell hoppings.

states. However, when a Hamiltonian $h(\mathbf{k})$ has an additional chiral symmetry, $\Pi h(\mathbf{k}) = -h(\mathbf{k})\Pi$ (for some chiral operator Π), zero energy states are concomitant to the topological phases having fractional charge $\frac{e}{2}$ [25]. In these cases the states are exponentially localized at the corners of the lattice, and are an important spectroscopic signature of the non-vanishing secondary invariant.

Disclinations. – We find that topological disclination defects that induce a curvature singularity in the lattice of our models also trap fractional charges. In Fig. 5 we show a disclination with a Frank angle of $-\frac{2\pi}{6}$ rad in the primitive model $h_{3c}^{(6)}$. Inducing such a disclination converts the hexagon of Fig. 3(d) into the pentagon of Fig. 5(a). The five corners in the pentagon result in an overall corner charge of $\frac{5e}{2}$. However, since the overall charge in the insulator must be an integer, we conclude that the core of the disclination must trap a fractional charge of $\frac{e}{2}$. Fig. 5(b) shows a plot of the charge density for the lattice in Fig. 5(a). As expected, the core of the disclination traps a fractional charge of $\frac{e}{2}$. Generalizing this principle of charge conservation (mod e), the index for the corner charge at the core of disclinations in a C_n symmetric insulator is

$$Q^{\text{disclination}} = -\frac{\Omega}{2\pi/n} Q^{\text{corner}} \bmod e. \quad (8)$$

Inducing this disclination disrupts the chiral symmetry in the primitive model $h_{3c}^{(6)}$. Thus, although the pristine insulator has zero energy modes localized at corners [25], there are no such states at the core of the disclination. Despite this, the fractional charge trapped at the core of the defect is robustly quantized to $\frac{e}{2}$, suggesting that disclinations are bulk probes of TIs with $Q^{\text{corner}} \neq 0$, just as dislocations are bulk probes of TIs with $\mathbf{P} \neq \mathbf{0}$ [26, 27].

Acknowledgements. – We thank Aris Alexandradinata,

Andrei Bernevig, and Eugeniu Plamadeala, for useful discussions. W.A.B. and T.L.H. thank the U.S. National Science Foundation under grant DMR-1351895 and the Sloan Foundation for support. TL thanks US National Science Foundation (NSF) Emerging Frontiers in Research and Innovation (EFRI) grant EFMA-1627184.

- [1] R. D. King-Smith and D. Vanderbilt, *Phys. Rev. B* **47**, 1651 (1993).
- [2] D. Vanderbilt and R. King-Smith, *Phys. Rev. B* **48**, 4442 (1993).
- [3] R. Resta, *Rev. Mod. Phys.* **66**, 899 (1994).
- [4] W. A. Benalcazar, B. A. Bernevig, and T. L. Hughes, *Science* **357**, 61 (2017).
- [5] W. A. Benalcazar, B. A. Bernevig, and T. L. Hughes, arXiv:1708.04230 (2017).
- [6] Y. Zhou, K. M. Rabe, and D. Vanderbilt, *Phys. Rev. B* **92**, 041102 (2015).
- [7] A. Altland and M. R. Zirnbauer, *Phys. Rev. B* **55**, 1142 (1997).
- [8] A. P. Schnyder, S. Ryu, A. Furusaki, and A. W. W. Ludwig, *Phys. Rev. B* **78**, 195125 (2008).
- [9] A. Kitaev, AIP Conference Proceedings **1134**, 22 (2009).
- [10] L. Fu, *Phys. Rev. Lett.* **106**, 106802 (2011).
- [11] C. Fang, M. J. Gilbert, and B. A. Bernevig, *Phys. Rev. B* **86**, 115112 (2012).
- [12] J. C. Y. Teo and T. L. Hughes, *Phys. Rev. Lett.* **111**, 047006 (2013).
- [13] W. A. Benalcazar, J. C. Y. Teo, and T. L. Hughes, *Phys. Rev. B* **89**, 224503 (2014).
- [14] J. Zak, *Phys. Rev. Lett.* **62**, 2747 (1989).
- [15] T. L. Hughes, E. Prodan, and B. A. Bernevig, *Phys. Rev. B* **83**, 245132 (2011).
- [16] A. M. Turner, Y. Zhang, R. S. Mong, and A. Vishwanath, *Phys. Rev. B* **85**, 165120 (2012).
- [17] B. Bradlyn, L. Elcoro, J. Cano, M. G. Vergniory, Z. Wang, C. Felser, M. I. Aroyo, and B. A. Bernevig, *Nature* **547**, 298 EP (2017).
- [18] H. C. Po, A. Vishwanath, and H. Watanabe, *Nature Communications* **8**, 50 (2017).
- [19] J. C. Y. Teo and C. L. Kane, *Phys. Rev. B* **82**, 115120 (2010).
- [20] A. Kitaev, *AIP Conf. Proc.* **1134**, 22 (2008).
- [21] N. Marzari and D. Vanderbilt, *Phys. Rev. B* **56**, 12847 (1997).
- [22] N. Marzari, A. A. Mostofi, J. R. Yates, I. Souza, and D. Vanderbilt, *Rev. Mod. Phys.* **84**, 1419 (2012).
- [23] W. P. Su, J. R. Schrieffer, and A. J. Heeger, *Phys. Rev. Lett.* **42**, 1698 (1979).
- [24] Z. Song, Z. Fang, and C. Fang, arXiv preprint: 1708.02952v1 (2017).
- [25] J. Noh, W. A. Benalcazar, S. Huang, M. J. Collins, K. P. Chen, T. L. Hughes, and M. C. Rechtsman, *Nature Photonics* (2018), 10.1038/s41566-018-0179-3.
- [26] J. C. Y. Teo and C. L. Kane, *Phys. Rev. B* **82**, 115120 (2010).
- [27] V. Jurićić, A. Mesaros, R.-J. Slager, and J. Zaanen, *Phys. Rev. Lett.* **108**, 106403 (2012).